

Efficient NO Calculations in Turbulent Non-Premixed Flames Using PDF Methods

Michael A. Wild^{*1}, Benjamin T. Zoller¹, Jonas Allegrini¹, Patrick Jenny¹

¹Institute of Fluid Dynamics, ETH Zurich, CH-8092 Zurich, Switzerland

Abstract

A new approach to NO modelling for non-premixed turbulent flames with transported joint probability density function (PDF) methods was developed. The NO formation rate obtained using a full mechanism is tabulated as a function of mixture fraction, scalar dissipation rate and NO concentration, thus taking into account backward reactions. The formation rate is then integrated along particle trajectories, subject to molecular mixing. Validation of the method was done with the Sandia flame D, for which good results were achieved.

Introduction

As environmental legislation becomes more stringent and since more than 80% of the primary energy is being produced by burning fossil fuel [1, 2], it is of increasing interest to understand and control the mechanisms taking place in combustion devices, both to increase their efficiency and to mitigate the emitted pollutants. Of special importance are emissions with strong impact on the environment. Nitric oxides (NO_x) for example are estimated to have a global warming potential (GWP) of 295 (i.e. 295 times higher than CO₂) over 100 years [3]. The reduction of these emissions can be facilitated by accurate NO production models.

The major challenge of turbulent reactive flow simulations arises from the huge range of length and time scales involved in the chemical and flow processes leading to a set of extremely stiff governing equations. However, if the chemical time scales are much smaller than those of the flow, the laminar flamelet approach can be employed [4, 5, 6]. There it is assumed that the embedded flame structure can be captured by one dimensional laminar flame solutions. For diffusion flames (with some additional assumptions) these laminar flamelets can be computed in mixture fraction space and are tabulated (temperature, species mass fractions etc.) as a function of mixture fraction and scalar dissipation rate. Flamelet models for non-premixed combustion have been extremely successful in predicting temperature and major species concentrations for a broad range of applications, but their usage for slow reactions (e.g. NO formation [7, 8, 9]) is more problematic, since the time scale associated with those slow processes are similar or larger than those of the flow. It was attempted to address this problem by tabulating the formation rates of these minor species instead of their equilibrium mass fractions as a function of mixture fraction and scalar dissipation rate, which can then be integrated along fluid particle trajectories to obtain the species concentrations [10, 11, 12]. However, this approach generally leads to an over-prediction of NO in the downstream region, since backward reactions are not properly taken into account and hence the NO concentration does not drift towards an equilibrium.

Specific Objectives

In this paper, a new NO formation model for non-premixed flames is proposed. It is based on the non-premixed laminar flamelet approach, where the NO-formation rates are tabulated as a function of not only the scalar dissipation rate and the mixture fraction, but also of the NO concentration. The method was tested within a PDF modelling framework, where a hybrid finite-volume (FV) / particle Monte Carlo method is employed to solve the joint velocity-composition-frequency probability density function (JPDF) transport equation efficiently [13, 14, 15, 16, 17]. A simulation study with the Sandia flame D [18] was performed to show the validity of the NO formation model.

PDF Modelling Framework

Our model was implemented in the hybrid finite volume / particle Monte Carlo PDF code PDF2DFV [19]. The Reynolds averaged Euler (RAE) equations with an energy source term, i.e.

$$\frac{\partial}{\partial t} \langle \rho \rangle + \frac{\partial}{\partial x_i} (\langle \rho \rangle \tilde{U}_i) = 0 \quad , \quad (1)$$

$$\begin{aligned} \frac{\partial}{\partial t} (\langle \rho \rangle \tilde{U}_i) + \frac{\partial}{\partial x_j} (\langle \rho \rangle \tilde{U}_i \tilde{U}_j + \langle p \rangle \delta_{ij}) \\ = - \frac{\partial}{\partial x_j} (\langle \rho \rangle \tilde{u}_i \tilde{u}_j) \quad \text{and} \end{aligned} \quad (2)$$

$$\begin{aligned} \frac{\partial}{\partial t} (\langle \rho \rangle \tilde{E}_s) + \frac{\partial}{\partial x_i} (\tilde{U}_i (\langle \rho \rangle \tilde{E}_s + \langle p \rangle)) \\ = \langle \rho \rangle \dot{Q} - \frac{\partial}{\partial x_i} (\langle \rho \rangle \tilde{u}_i \tilde{h}_s) \\ - \frac{\partial}{\partial x_i} \left(\frac{\langle \rho \rangle}{2} \tilde{u}_i \tilde{u}_j \tilde{u}_j \right) - \frac{\partial}{\partial x_i} (\tilde{U}_j \langle \rho \rangle \tilde{u}_i \tilde{u}_j) \end{aligned} \quad (3)$$

are solved simultaneously together with the modelled joint fluctuating velocity-frequency-composition probability density function equation

* Corresponding author: wild@ifd.mavt.ethz.ch

$$\begin{aligned}
& \frac{\partial \langle \rho \rangle f}{\partial t} + \frac{\partial}{\partial x_j} \left((\bar{U}_j + v_j) \langle \rho \rangle f \right) - \frac{\partial \bar{U}_i}{\partial x_j} \frac{\partial}{\partial v_i} (v_j \langle \rho \rangle f) \\
& + \frac{1}{\langle \rho \rangle} \frac{\partial}{\partial x_j} \left(\langle \rho \rangle \overline{u_i u_j} \right) \frac{\partial \langle \rho \rangle f}{\partial v_i} \\
& = \frac{\partial}{\partial v_i} \left(\left(\frac{1}{2} + \frac{3}{4} \right) \Omega v_i \langle \rho \rangle f + \frac{1}{2} C_0 k \Omega \frac{\partial \langle \rho \rangle f}{\partial v_i} \right) \quad (4) \\
& - \frac{\partial}{\partial \Psi_\alpha} \left(\left\langle \frac{D\phi_\alpha}{Dt} \middle| \mathbf{v}, \Theta, \Psi; \mathbf{x}, t \right\rangle \langle \rho \rangle f \right) \\
& - \frac{\partial}{\partial \Theta} \left(\left\langle \frac{D\omega}{Dt} \middle| \mathbf{v}, \Theta, \Psi; \mathbf{x}, t \right\rangle \langle \rho \rangle f \right) ,
\end{aligned}$$

where the simplified Langevin model (SLM) is employed [20].

The variables ρ , \mathbf{U} , E_s , h_s and p represent fluid density, flow velocity, sensible total energy, sensible enthalpy and pressure, respectively. The operators $\langle \cdot \rangle$, $\langle \cdot \rangle$ and $\bar{\cdot}$ denote conditional expectations, Reynolds and Favre averaged quantities, and f is the joint PDF of the fluctuating velocity $\mathbf{u} = \mathbf{U} - \bar{\mathbf{U}}$, the turbulence frequency ω and the composition Φ_α . The independent variables \mathbf{v} , Θ and Ψ_α are the sample space coordinates of \mathbf{u} , ω and Φ_α , respectively. The model constant C_0 is set to 2.13. In the hybrid solution algorithm, the mass density function $\mathcal{F} = \langle \rho \rangle f$ is represented by a cloud of many particles, which are evolved consistently in the \mathbf{x} - \mathbf{v} - Θ - Ψ -space [19].

The right hand sides of Eqs. (2) and (3), the turbulent kinetic energy $k = \overline{u_i u_i} / 2$ and the conditional frequency $\Omega = C_\Omega \langle \rho \omega | \Theta > \bar{\omega} \rangle / \langle \rho \rangle$ can be computed from \mathcal{F} . The conditional expectation $\left\langle \frac{D\phi_\alpha}{Dt} \middle| \mathbf{v}, \Theta, \Psi; \mathbf{x}, t \right\rangle$ describes the average “velocity” in composition space due to chemical reactions and molecular diffusion. While the former appears in closed form, the latter is described with a mixing model; here with the interaction by exchange with the mean (IEM) model [21] with the model constant C_ϕ set to the increased value of 2.5 (compared to the standard value of 2.0 for inert flows). To close the conditional expectation $\left\langle \frac{D\omega}{Dt} \middle| \mathbf{v}, \Theta, \Psi; \mathbf{x}, t \right\rangle$, the Gamma distribution model [20, section 12.5.3] is used.

Such a joint PDF method has the advantage that turbulent convection and the reaction source term appear in closed form and with this hybrid solution algorithm the PDF transport equation can be solved quite efficiently.

Combustion Modelling

To calculate the statistics of the embedded flame structure, the laminar flamelet approach is combined with the PDF method described above. The flame tables are computed using the open source software Cantera [22] with the reaction mechanisms GRI 2.11 and GRI 3.0 [23]. However, as discussed in the introduction, such flamelet modelling relies on scale separation, which is not justified for some of the slow reactions responsible for NO production. Here, a new and efficient modelling approach for NO formation in non-premixed turbulent flames is described.

It is assumed that for a given scalar dissipation rate diffusion and chemistry are in equilibrium for all species other than NO. This is based on the assumption that NO is formed much slower than the other species and that the radical concentrations are insensitive to the NO mechanism. Evidence for the latter assumption comes from studies with humid air at 2300 K. These have shown that NO production affects the OH concentration only by a few percent and the same is true for other radicals.

In existing diffusion flamelet models, the NO source term is tabulated as a function of mixture fraction and scalar dissipation rate [10, 11, 12, 24]. However, such models predict an NO formation rate independent of the NO level, which is wrong and leads to an over-prediction; primarily in regions far downstream of the flame. Chou et al. [25] proposed a model where the NO formation is proportional to the NO concentration. This assumption, however, is only valid for simplified NO chemistry.

We developed a new approach in which the NO formation rate is not only tabulated as a function of mixture fraction and scalar dissipation rate, but also depends on the NO concentration. With this model, the NO concentration drifts to an equilibrium value, which is consistent with the reality, but in contrast to existing approaches. In the context of our PDF simulations (which delivers the joint mixture fraction, scalar dissipation rate, NO concentration statistics), the NO concentration of a Lagrangian particle evolves according to the IEM mixing model and the tabulated formation rate. Note that the latter depends on the particle’s mixture fraction, scalar dissipation rate and the NO concentration. All other species mass fractions and the enthalpy depend on the mixture fraction and the scalar dissipation rate only and are obtained from conventional flamelet-table look-ups. The computational cost of this method is only marginally higher than that of classical diffusion flamelet models, which is primarily due to an additional time step restriction imposed by the NO formation rate.

To obtain the NO source term, the stationary flamelet equation is solved at various scalar dissipation rates. Since the other species and the temperature are virtually insensitive to NO variations, it is justified to vary the NO concentration independently. Thus it is straight forward to extract realistic NO formation rates from a converged stationary flamelet solution for a wide range of NO concentrations by artificially imposing the NO mass fraction and then extracting the corresponding NO formation rate. Figure 1 shows the strong dependence of the NO source term on the NO concentration for a stationary flamelet solution which has been computed for the Sandia flame D case using the GRI 2.11 (top) and GRI 3.0 (bottom) mechanisms at a scalar dissipation rate of $\chi = 0.1 \text{ s}^{-1}$. One can observe a large discrepancy between the solutions obtained with the two mechanisms. It was shown previously [26] that the GRI 3.0 mechanism significantly over-predicts NO production, albeit it exhibits a better

overall performance. The flame kinetics is almost identical for both mechanisms. This is the reason why only the GRI 2.11 mechanism was employed for the following validation study.

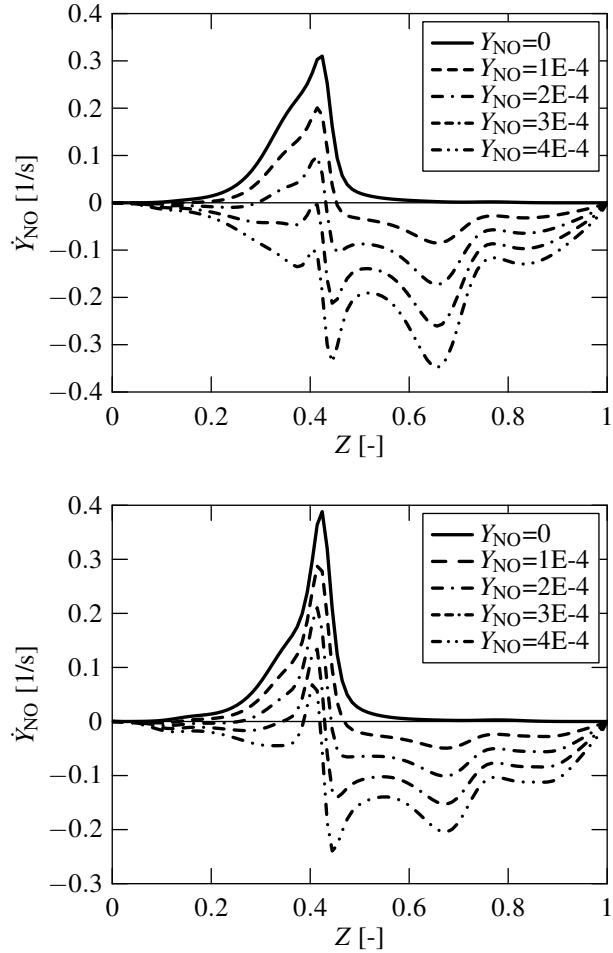


Figure 1: NO formation rate \dot{Y}_{NO} as a function of mixture fraction and NO mass fraction extracted from a stationary flamelet solution using the GRI 2.11 (top) and GRI 3.0 (bottom) mechanisms.

Results and Discussion

To test our new model for NO formation in non-premixed turbulent flames, the Sandia National Laboratories flame D [18] was considered. It is a piloted jet flame with a jet diameter of $d = 7.2$ mm, which has a low degree of local extinction. Temperature and velocity fields were computed by the hybrid PDF method mentioned above combined with a simple flamelet model [4, 5, 6]. NO formation was obtained from the model presented in the previous section. Both flamelet and NO formation tables were calculated with Cantera and the GRI 2.11 mechanism. In the PDF simulation, the NO formation was computed for each particle according to the tabulated formation rates. Note that mixture fraction, scalar dissipation rate and the NO concentration are particle properties. Molecular mixing of NO and mixture fraction is described by the IEM mixing model. We used 60 cells both in axial and radial direction with strong refinement near

the symmetry axis and at the inlet. In average 30 computational particles were employed per cell. The relatively low number of particles is compensated by employing a moving time-averaging method.

Figures 2, 3, 4 and 5 show radial profiles of the mean axial velocity \bar{U} , the mean temperature \bar{T} , the mean mixture fraction \bar{Z} and the RMS mixture fraction Z_{RMS} , respectively, at four downstream positions. The lines represent the PDF simulation results and the symbols are measured data points [18]. As can be seen, the agreement with the experimental data is very good for all the quantities at all downstream positions. Only at $x/d = 45$ the mean temperature, the mean mixture fraction and the RMS mixture fraction are slightly over-predicted, whereas the axial velocity is under-predicted.

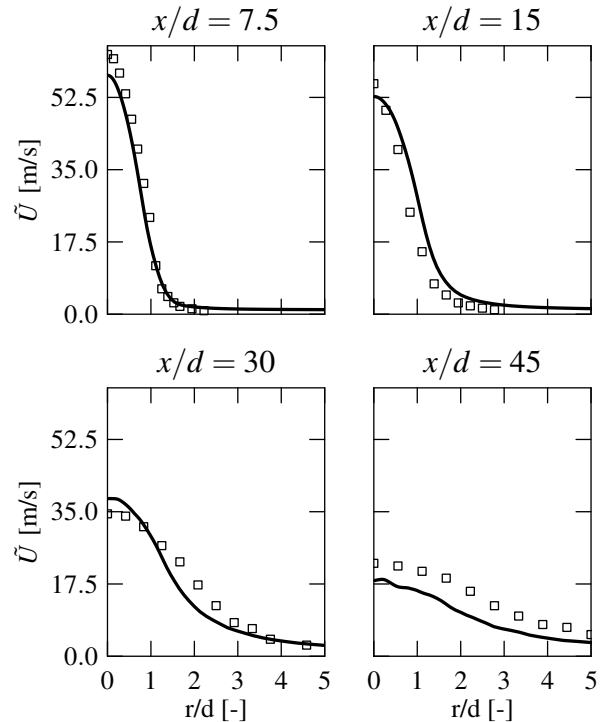


Figure 2: Radial profiles of the mean axial velocity \bar{U} at various downstream positions, showing the results obtained with the hybrid PDF method (solid line) and the experimental data points (symbols).

Radial profiles of the RMS temperature T_{RMS} are depicted in Fig. 6. It can be observed that the general shape is captured well. The extrema, however, deviate from the experimental results. Near the centre-line T_{RMS} is over-predicted at the first three downstream positions, whereas the profile is shifted away from the symmetry axis at $x/d = 45$.

In Figures 7, 8 and 9 radial profiles of the Reynolds stresses $\overline{u'u'}$, $\overline{v'v'}$ and $\overline{u'v'}$ are displayed. It can be seen that the peak value of $\overline{u'u'}$ is under-predicted at the downstream positions $x/d = 7.5$ and $x/d = 15$, but then is too high at $x/d = 30$. The peak value of $\overline{v'v'}$ is slightly over-predicted at all downstream positions and at $x/d = 30$ and $x/d = 45$ the profile is too narrow. Lastly, $\overline{u'v'}$ matches the experimental data well at the first two downstream positions,

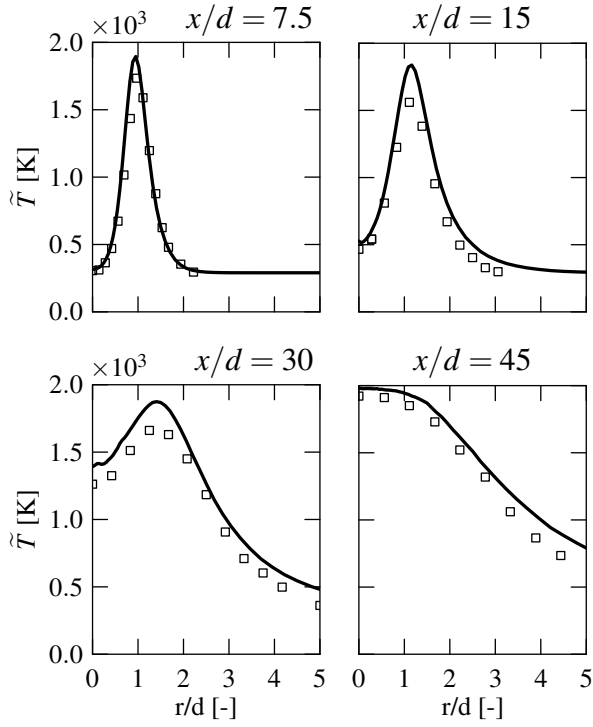


Figure 3: Radial profiles of the mean temperature \tilde{T} at various downstream positions, showing results obtained with the hybrid PDF method (solid line) and the experimental data points (symbols).

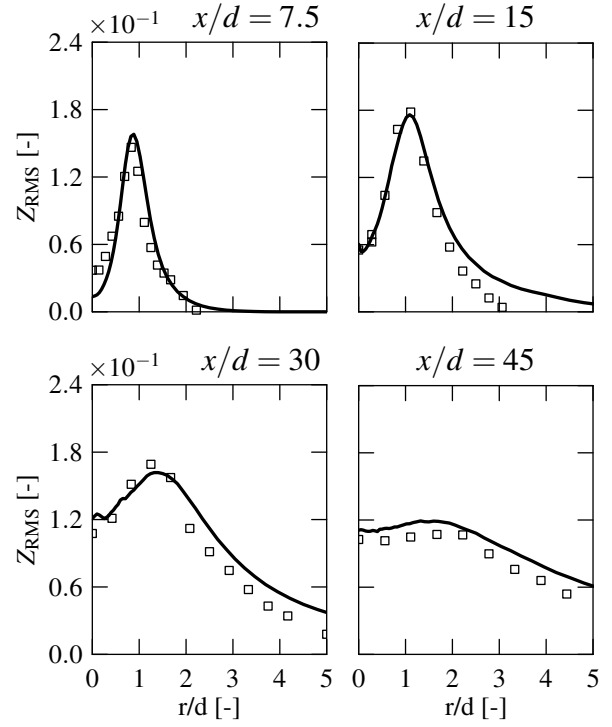


Figure 5: Radial profiles of the RMS mixture fraction Z_{RMS} at various downstream positions, showing the results obtained with the hybrid PDF method (solid line) and the experimental data points (symbols).

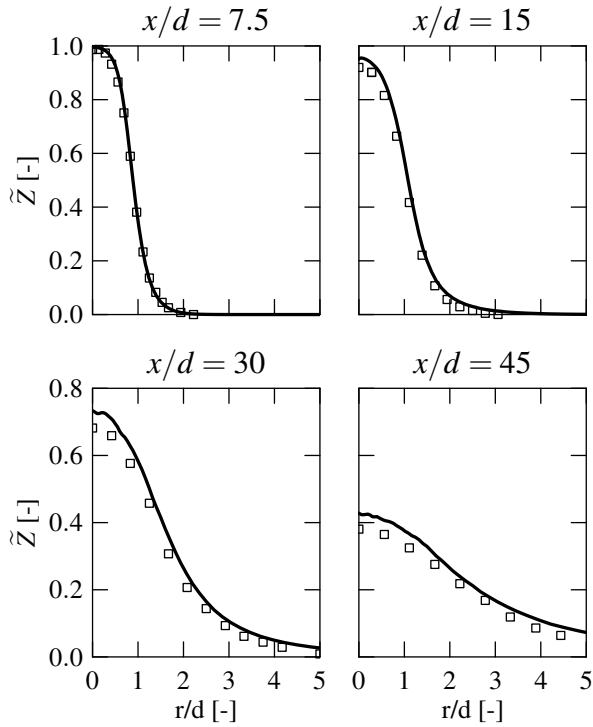


Figure 4: Radial profiles of the mean mixture fraction \tilde{Z} at various downstream positions, showing the results obtained with the hybrid PDF method (solid line) and the experimental data points (symbols).

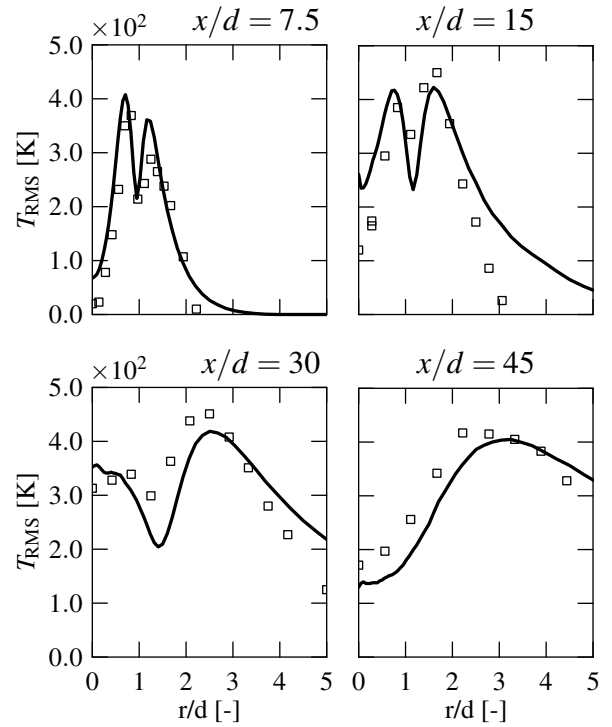


Figure 6: Radial profiles of the RMS temperature T_{RMS} at various downstream positions, showing results obtained with the hybrid PDF method (solid line) and the experimental data points (symbols).

but over-predicts the peak value at $x/d = 30$ and the profile is also shifted towards the centre-line. At $x/d = 45$ the peak value matches the experimental data again, but the profile still shows an offset towards the centre-line.

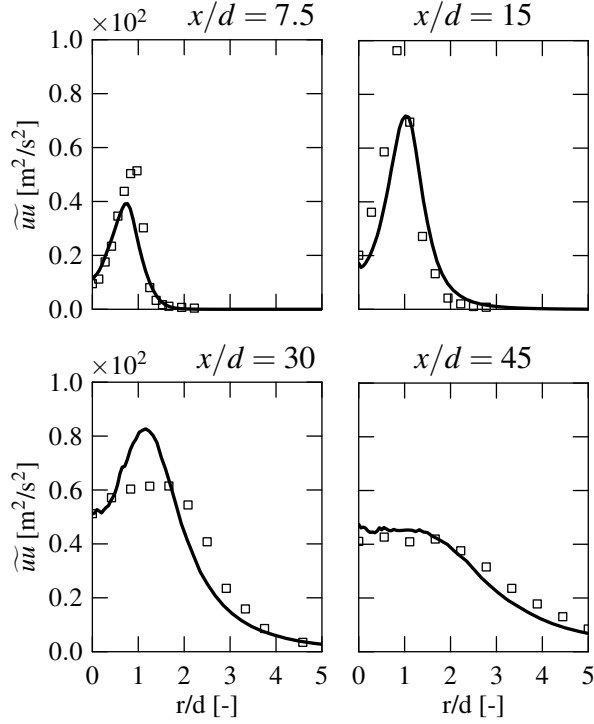


Figure 7: Radial profiles of the \overline{uu} Reynolds stress at various downstream positions, showing the results obtained with the hybrid PDF method (solid line) and the experimental data points (symbols).

In Fig. 10, radial NO profiles at the same downstream positions are depicted. Again, the solid lines are the PDF simulation results using the NO formation model presented in this paper and the symbols mark the experimental data. The dashed line represents the results reported by Wang et al. [27], who used a hybrid finite volume / composition PDF method combined with an eddy viscosity turbulence model (multi-time-scale $k-\varepsilon$ [28]). In their simulations the flow was modeled by solving the parabolized Navier-Stokes (PNS) equations [29], where only the axial momentum equation was solved; the radial component was deduced from the continuity equation. The joint scalar PDF transport equation was solved using the node-based Monte Carlo particle method developed by Pope [30], where the transport in radial direction due to turbulent fluctuations was closed by the gradient diffusion assumption [31, 32]. In their studies, the GRI 3.0 reaction mechanism was integrated for each individual particle and radiative heat transfer was neglected. For molecular mixing, the Euclidean minimum spanning tree (EMST) [33] mixing model was employed. The plots in Fig. 10 show that our new approach, which is computationally much cheaper than the one used by Wang et al., gives comparable results. One can observe that our NO mass fraction results are invariably too high by a factor of 2, which we find to be quite remarkable. For illus-

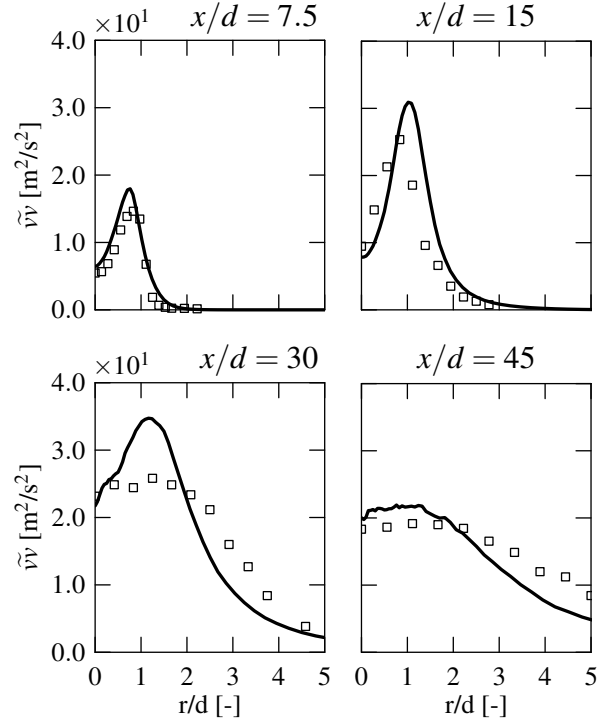


Figure 8: Radial profiles of the \overline{vv} Reynolds stress at various downstream positions, showing the results obtained with the hybrid PDF method (solid line) and the experimental data points (symbols).

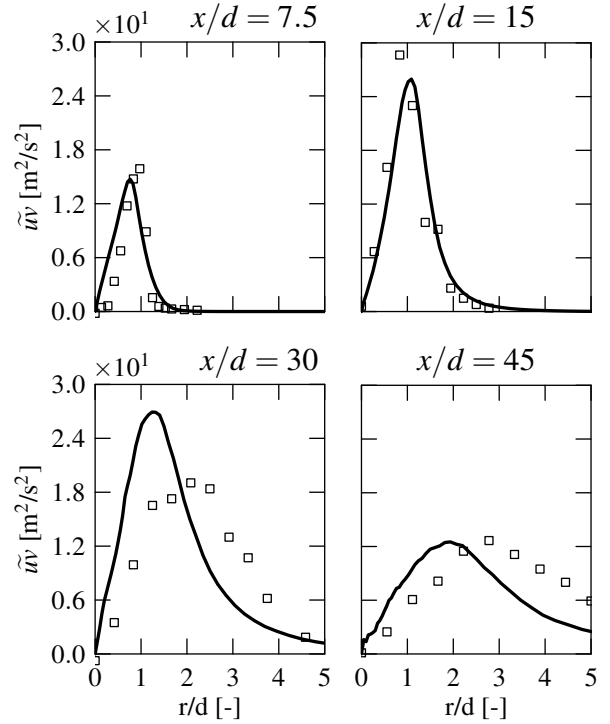


Figure 9: Radial profiles of the \overline{uv} Reynolds stress at various downstream positions, showing the results obtained with the hybrid PDF method (solid line) and the experimental data points (symbols).

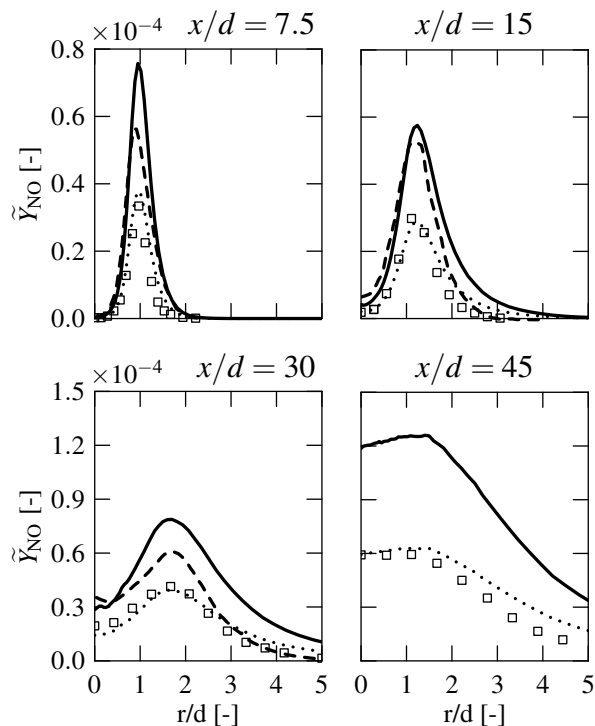


Figure 10: Radial profiles of the mean NO mass fraction \bar{Y}_{NO} at various downstream positions, showing the results obtained with our new method (solid line), our results scaled by a factor of 0.5 (dotted line), the values reported by Wang et al. [27] using detailed chemistry (dashed line) and the experimental data points (symbols).

tration we included the quantity $Y_{\text{NO}}/2$ (dotted line) in Fig. 10, which matches the experimental data strikingly well. This systematic over-prediction by an almost constant factor of about 2 is not understood yet.

Conclusions

A new model for NO prediction in turbulent non-premixed combustion based on three-dimensional flamelets was devised. Different than in previous methods similar to the one presented here, the NO source term also depends on the NO concentration, i.e. it is extracted from stationary flamelet solutions for different NO mass fractions. Here, molecular mixing of NO and mixture fraction was treated with the IEM mixing model. Validation of the model was performed for the Sandia flame D and the results are competitive with those obtained from PDF simulations using direct integration of complex mechanisms. However, the required CPU time for the simulations with the new method is only a few percent higher than that of standard PDF/flamelet simulations. On the other hand it has been reported e.g. by Raman et al. [34] that more than 90% of the CPU time is spent for the reactions, if direct integration together with in situ adaptive tabulation (ISAT) [35] is employed.

Currently we do not understand the reason for the systematic over-prediction of the NO concentration by an almost constant factor of 2 and further investigations are necessary.

It remains to be mentioned that the method presented in this paper has similarities to progress variable approaches for non-premixed combustion in conventional finite volume methods and therefore this new approach should be applicable for such frameworks.

References

- [1] IEA (Ed.), Key World Energy Statistics 2004, International Energy Agency, 2004.
- [2] IEA (Ed.), Key World Energy Statistics 2007, International Energy Agency, 2007.
- [3] O. e. a. Boucher, The Climate Change 2001: The Scientific Basis, Cambridge University Press, 2001, Ch. 6, p. 388.
- [4] N. Peters, *Progr Energ Combust Sci* 10 (1984) 319–339.
- [5] N. Peters, *Proc Combust Inst* 21 (1) (1986) 1231–1250.
- [6] N. Peters, *Turbulent Combustion*, Cambridge University Press, 2000.
- [7] Y. B. Zeldovich, P. Y. Sadovnikov, D. A. Frank-Kamenetskii, Academy of Sciences of UDSSR, Moscow.
- [8] C. P. Fenimore, *Proc Combust Inst* 13 (1971) 373–380.
- [9] J. A. Miller, C. T. Bowman, *Progr Energ Combust Sci* 15 (1989) 287–338.
- [10] J. Y. Chen, W.-C. Chang, *Proc Combust Inst* 26 (1996) 2207–2214.
- [11] A. Heyl, H. Bockhorn, *Chemosphere* 42 (2001) 449–462.
- [12] J. P. H. Sanders, J. Y. Chen, I. Gokalp, *Combust Flame* 111 (1997) 1–15.
- [13] P. Jenny, M. Muradoglu, K. Liu, S. B. Pope, D. A. Caughey, *J Comput Phys* 169 (1) (2001) 1–23.
- [14] B. Rembold, P. Jenny, in: *AIAA Comput Fluid Dynam*, 2005, pp. 1–11.
- [15] B. Rembold, P. Jenny, *J Comput Phys* 220 (2006) 59–87.
- [16] B. Rembold, M. Grass, P. Jenny, *Comput Fluid* 37 (3) (2008) 181–193.
- [17] M. Muradoglu, P. Jenny, S. B. Pope, D. A. Caughey, *J Comput Phys* 154 (2) (1999) 342–371.
- [18] R. Barlow. Sandia National Laboratories TNF Workshop <http://www.ca.sandia.gov/TNF>.
- [19] P. Jenny, S. B. Pope, M. Muradoglu, D. A. Caughey, *J Comput Phys* 166 (2001) 218–252.
- [20] S. B. Pope, *Turbulent flows*, Cambridge University Press, Cambridge, 2000.
- [21] C. Dopazo, E. E. O’Brien, *Acta Astronautica* 1 (9-10) (1974) 1239–1266.
- [22] D. G. Goodwin. Cantera <http://www.cantera.org>.
- [23] G. P. Smith, D. M. Golden, M. Frenklach, N. W. Moriarty, B. Eiteneer, M. Goldenberg, C. T. Bowman, R. K. Hanson, S. Song, W. C. J. Gardiner, V. V. Lissianski, Z. Qin. GRI Mech http://www.me.berkeley.edu/gri_mech/.
- [24] D. V. Volkov, A. A. Belokin, D. A. Lyubimov, V. M. Zakharov, G. Opydke, *J Eng Gas Turbine Power* 123 (19) (2001) 774–778.
- [25] C.-P. Chou, J.-Y. Chen, C. G. Yam, K. D. Marx, *Combust Flame* 114 (3-4) (1998) 420–435.
- [26] R. R. Cao, S. B. Pope, *Combust Flame* 143 (2005) 450–470.
- [27] H. Wang, Y. Chen, *Chem Eng Sci* 59 (2004) 3477–3490.
- [28] S.-W. Kim, C.-P. Chen, *Numerical Heat Transfer Part B* 16 (1989) 193–211.
- [29] S. G. Rubin, J. C. Tannehill, *Annual Review of Fluid Mechanics* 24 (1) (1992) 117–144.
- [30] S. B. Pope, *Combustion Science and Technology* 25 (5) (1981) 159–174.
- [31] S. B. Pope, *Progr Energ Combust Sci* 11 (2) (1985) 119–192.
- [32] R. Lindstedt, S. Louloudi, E. Váos, *Proc Combust Inst* 28 (1) (2000) 149–156.
- [33] S. Subramaniam, S. B. Pope, *Combust Flame* 117 (4) (1999) 732–754.
- [34] V. Raman, R. O. Fox, A. D. Harvey, *Combust Flame* 136 (2004) 327–350.
- [35] S. B. Pope, *Combust Sci Tech* 1 (1) (1997) 41–63.